EEG Alpha Power Modulation
of fMRI Resting-State Connectivity

René Scheeringa,[1–3] Karl Magnus Petersson,[1,4,5] Andreas Kleinschmidt,[2,3]
Ole Jensen,[1] and Marcel C.M. Bastiaansen[1,4]

Abstract

In the past decade, the fast and transient coupling and uncoupling of functionally related brain regions into networks has received much attention in cognitive neuroscience. Empirical tools to study network coupling include functional magnetic resonance imaging (fMRI)-based functional and/or effective connectivity, and electroencephalography (EEG)/magnetoencephalography-based measures of neuronal synchronization. Here we use simultaneously recorded EEG and fMRI to assess whether fMRI-based connectivity and frequency-specific EEG power are related. Using data collected during resting state, we studied whether posterior EEG alpha power fluctuations are correlated with connectivity within the visual network and between the visual cortex and the rest of the brain. The results show that when alpha power increases, BOLD connectivity between the primary visual cortex and occipital brain regions decreases and that the negative relation of the visual cortex with the anterior/medial thalamus decreases and the ventral–medial prefrontal cortex is reduced in strength. These effects were specific for the alpha band, and not observed in other frequency bands. The decreased connectivity within the visual system may indicate an enhanced functional inhibition during a higher alpha activity. This higher inhibition level also attenuates long-range intrinsic functional antagonism between the visual cortex and the other thalamic and cortical regions. Together, these results illustrate that power fluctuations in posterior alpha oscillations result in local and long-range neural connectivity changes.

Key words: alpha; EEG; fMRI; PPI; resting state

Introduction

THE PAST FEW YEARS several studies using simultaneously recorded electroencephalography (EEG) and functional magnetic resonance imaging (fMRI) have addressed the relation between EEG power and the blood oxygenation level dependent (BOLD) signal. These EEG-fMRI studies have predominantly investigated, where in the brain EEG power fluctuations correlate with the BOLD signal in both resting state (de Munck et al., 2009; Goldman et al., 2002; Laufs et al., 2003a, 2003b; Mantini et al., 2007; Moosmann et al., 2003; Scheeringa et al., 2008;) and task contexts (Hanslmayr et al., 2011b; Sammer et al., 2007; Scheeringa et al., 2009, 2011). Within these studies, the interest has focused mostly on the local BOLD correlates of alpha power.

Besides conventional analyses that investigate task-related changes in the strength of the BOLD signal, fMRI also offers the possibility to investigate the connectivity in the BOLD signal between different brain regions. In task settings, this can be studied by methods, including the psycho–physiological interaction (PPI) (Friston et al., 1997) and dynamic causal modeling (Friston et al., 2003), while in resting-state studies, correlational methods (Biswal et al., 1995; Fox et al., 2005) and independent component analysis are often used (Damoiseaux et al., 2006). However, the relationship between fMRI connectivity and electrophysiological phenomena is largely uncharted territory. Here, we explore how fMRI connectivity of visual regions both within those regions, and between the visual cortex and other brain regions as a function of posterior EEG alpha power.

[1]Donders Institute for Brain Cognition and Behaviour, Centre for Cognitive Neuroimaging, Radboud University Nijmegen, Nijmegen, The Netherlands.
[2]INSERM, Unité 992, Gif-sur-Yvette, France.
[3]NeuroSpin, I2BM, DSV, CEA, Gif-sur-Yvette, France.
[4]Max Planck Institute for Psycholinguistics, Nijmegen, The Netherlands.
[5]Department of Psychology, IBB/CBME, University of Algarve, Faro, Portugal.

We focus on the visual system because this network is reliably observed in resting-state fMRI studies (Damoiseaux et al., 2006; Mantini et al., 2007). More importantly, the strongest alpha oscillations are recorded from the posterior parts of the scalp and have been linked to visual processing. The source of these alpha oscillations is most likely located in the early visual cortex (Hoogenboom et al., 2006; Makeig et al., 2004a, 2004b). The visual system and the posterior alpha rhythm are therefore well-suited to explore how changes in fMRI connectivity relate to changes in EEG power.

Historically, alpha oscillations have been thought of as an idling rhythm, indicating inactivity of brain regions (Pfurtscheller et al., 1996). More recently, the view has changed toward a functional role of alpha oscillation in inhibiting neural task irrelevant regions (Klimesch et al., 2007; Mazaheri and Jensen, 2010). Both views lead to the hypothesis that increased strength of alpha oscillations in a brain region is related to the decreased connectivity with other brain regions. On the other hand, the fact that alpha oscillations dominate the EEG over the posterior scalp suggests that a large part of the visual cortex is involved in the generation. This large-scale alpha-band synchronization could be expressed in the increased connectivity within the visual system.

To test these two hypotheses, we used simultaneously recorded resting-state EEG and fMRI data. By using a PPI approach, we test whether connectivity of the primary visual cortex with other regions inside and outside the visual system differs for high versus low posterior alpha power originating from the early visual cortex. The posterior alpha rhythm originating from the early visual cortex was isolated by applying independent component analysis on the EEG data, and selecting the central posterior component (Makeig et al., 2004a, 2004b). With the PPI, we test whether the regression slope between brain regions differs between conditions. If alpha oscillations are indeed related to idling or inhibition of task-irrelevant regions, this would result in a reduced information flow between brain regions and consequence a lower regression slope between brain regions. This would not be expected if both regions are directly involved in the generation of alpha. In this case, alpha power would be related to a stronger alpha-phase synchrony between regions, which would indicate a stronger corticocortical interaction, or a common thalamocortical drive (Hughes and Crunelli, 2005; Saalmann and Kastner, 2011).

Methods

Subjects

Twenty right-handed volunteers (17 female, 3 male, age range: 18–28) participated in the study after giving written informed consent. None had a neurological impairment, experienced neurological trauma, or had used psychoactive medicines or drugs. The subjects were paid a small fee for their participation. The experiment was approved by a local ethics committee (CMO region Arnhem/Nijmegen).

Design and procedure

First, the electrode cap was applied and instructions were given. While in the scanner, the subjects first participated in a working memory experiment for approximately 1 h, divided in three blocks (see Scheeringa et al., 2009, for further details). Then, a resting-state measurement was carried out in which subjects were asked to watch a black fixation cross presented on a gray background for 10 min. At the end of the scanning sessions, a T1-weighted anatomical MRI was acquired. Between measurements, there were short breaks of a few minutes. Subjects were also allowed to leave the scanner during these breaks. Only the data from the 10-min resting-state measurement are used in the analysis presented here. Other findings from this data set have previously been reported in Scheeringa et al. (2008).

Electrophysiological recordings

EEG was recorded at 29 scalp sites (Fp1, Fp2, F3, F4, C3,C4, P3, P4, O1, O2, F7, F8, T7, T8, P7, P8, Fz, Cz, Pz, FC1,FC2, CP1, CP2, FC5, FC6, CP5, CP6, TP9, and TP10) with a MR-compatible BrainAmp MR amplifier (Brainproducts, Munich, Germany) and a custom-made MR-compatible electrode cap equipped with carbon wired sintered Ag/AgCl electrodes (Easycap, Herrsching-Breitbrunn, Germany). The reference electrode was located at FCz. To record the vertical EOG, one electrode was placed under the right eye. The ECG was measured by two dedicated electrodes attached to the electrode cap. One electrode was placed on the sternum; the other electrode was placed on the clavicle, near the shoulder. A 250-Hz hardware filter was placed between the electrode cap and the amplifier. The EEG was recorded with a 0.16 s time constant and a 100-Hz low-pass software filter, and continuously sampled at 5 kHz. Impedances were kept under 5 kΩ. Current limiting resistors were not part of the carbon-wired electrodes. All recordings were done with Brain Vision Recorder software (Brainproducts).

Image acquisition

MRI measurements were performed on a 1.5 T Sonata whole-body scanner (Siemens, Erlangen, Germany). Functional images were acquired using a gradient echo EPI sequence (TR 2.34 s, including a 50 ms gap between volume acquisitions; field of view = 224 mm, TE = 30 ms, 90° flip angle, 33 slices, 3.0-mm slice-thickness with 0.5-mm slice-gap; resulting in an isotropic voxel size of $3.5 \times 3.5 \times 3.5$ mm).

MR artifact removal EEG

The EEG data were corrected for gradient and pulse artifacts along the lines described by Allen and associates (1998, 2000) using the Vision Analyzer (Brainproducts). A 20-volume, baseline corrected sliding average was used for the correction of the gradient artifacts. After gradient correction, the data were low-pass filtered at 100 Hz and downsampled to 500 Hz. The average pulse artifact was calculated based on a sliding average, time locked to the R-peak present in the bipolar derivation of the two ECG electrodes. This sliding average was scaled to an optimum least squares fit for each heart beat using the scaling option in the Vision Analyzer before it was subtracted from the data. The data were subsequently re-referenced to a common average reference. The original reference channel was recomputed as FCz.

fMRI preprocessing

Processing of the fMRI data was carried out in SPM8. The fMRI data were corrected for movements and slice

acquisition time differences, anatomically normalized to the canonical EPI template provided by SPM8, downsampled to 2×2×2-mm resolution and smoothed with an isotropic Gaussian kernel (FWHM = 8 mm).

Alpha power extraction

Alpha power was estimated based on the central posterior alpha component that is reliably observed when independent component analysis is applied to EEG data (Makeig et al., 2002, 2004a, 2004b). Source analysis has indicated that the primary visual cortex is the most likely source of this component (Makeig et al., 2002, 2004a). Here we applied extended info-max independent component analysis (ICA) (Lee et al., 1999) as implemented in EEGLab 6.01 (Delorme and Makeig, 2004) on 7–13-Hz band-pass-filtered EEG data. Since many brain and artifact processes occur at specific frequencies (e.g., the medial frontal theta component and residual MR gradient artifacts), band-pass filtering before applying ICA increases the reliability of observing the central posterior alpha component. For each subject, one posterior alpha component was selected based on the following criteria: it should have (1) a peak in the alpha range (8–12 Hz) after the unmixing weights are applied on the unfiltered data (see also Scheeringa et al., 2011 for a similar approach) and (2) a central–posterior topography of the mixing weights, which expresses the relative strength each component time course is expressed at each electrode. The average power spectrum of the selected components was based on power spectra computed from FFTs applied on Hanning tapered 2s windows of the component time courses using the Fieldtrip toolbox (Oostenveld et al., 2011). These settings result in a resolution of the spectra of 0.5 Hz. These 2s windows were shifted in 0.1-s steps. To be able to show the spectrum outside the alpha range, the unmixing weights were applied on the unfiltered EEG data before the spectrum was calculated. The average topography and power spectrum of the selected components are depicted in Fig. 1.

Connectivity analysis

Previous work has shown that the posterior alpha power component is likely generated in the primary visual cortex (Makeig et al., 2002, 2004a, 2004b) and is inversely related to the BOLD signal close to source location (Scheeringa et al., 2011). We therefore chose to base the selection of the seed region on a correlation analysis between power fluctuations in the posterior component and early visual cortex. Alpha power correlated negatively with the BOLD signal in the visual cortex. A part of the region that was correlated negatively with the BOLD signal, and that was for the largest part within the primary visual cortex (anatomy toolbox) (Eickhoff et al., 2005) (for further details see below), was selected as seed for the PPI analysis. We also computed standard functional connectivity estimates of this seed region with the rest of the brain, to establish which brain regions are connected to the seed region in the primary visual cortex.

Alpha-BOLD correlation analysis

For the alpha power-BOLD correlation analysis, we followed an EEG informed fMRI analysis approach (Debener et al., 2006). The construction of the alpha power regressor was based on a 4-Hz band centered around the individual alpha peak (mean 9.73 Hz, standard deviation 1.15 Hz) observed in the average spectrum of the selected independent component. Power was averaged over the four frequency bins (of 0.5 Hz each) below the peak frequency, the peak frequency bin and the 3 bins above, resulting in a 10-min power time course with a 0.1-s resolution. An EEG-based power regressor was formed from this time course by subsequently z-transforming the values for normalization, convolution with the hemodynamic response implemented in SPM8 (www.fil.ion.ucl.ac.uk/spm), and downsampling to one value for each scan. Together with nuisance variables consisting of the six realignment parameters and four compartment signals (modeling the average signal in the gray matter, white matter, cerebrospinal fluid, and outside the brain), this alpha power regressor formed the design matrix for the analysis using the general linear model implemented in SPM8. The compartment signal averages were based on the segmented individual anatomical images (Ashburner and Friston, 2005).

At group level, the parameter estimates for the alpha power-based regressor were tested against zero in a single-sample t-test. Significance was assessed using the Gaussian random field correction for multiple nonindependent
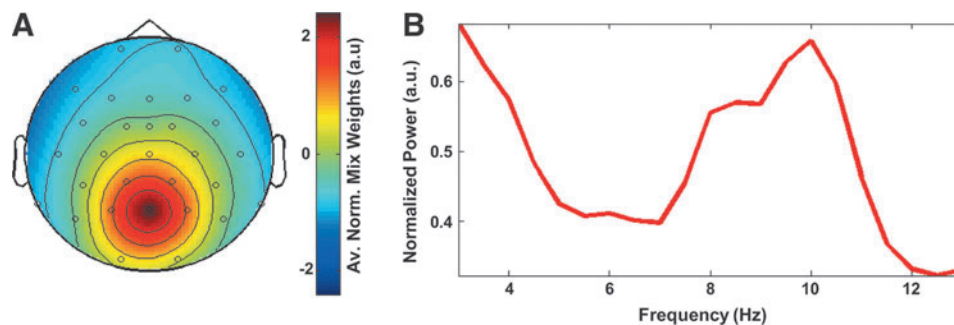

FIG. 1. Average topography **(A)** and power spectrum **(B)** of the independent components selected for further analyses. The topography is based on the individual root mean square normalized topographies of the independent component analysis (ICA) mixing weights. These weights describe the relative strength and polarity at which the time course of a component is projected onto the electroencephalography (EEG) channels. The single-subject power spectra that constitute the average spectrum were calculated after the ICA unmixing weights were applied on the unfiltered EEG data. The power spectrum was averaged after normalizing the single-subject spectra to the maximum in the alpha-frequency range (8–12 Hz).
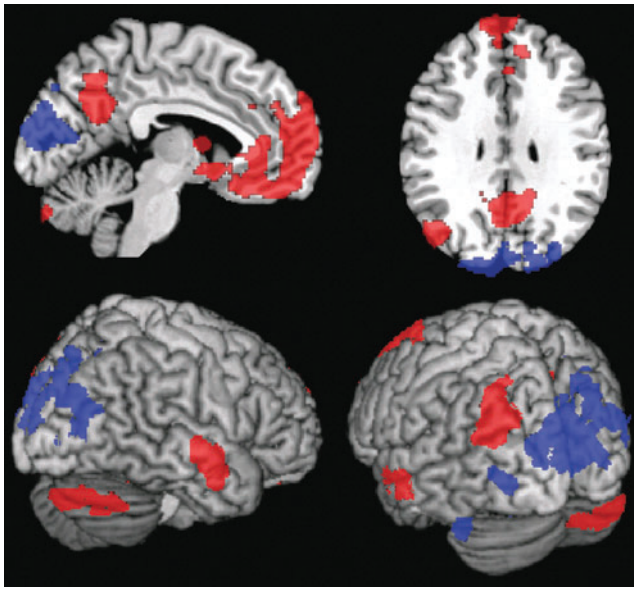
FIG. 2. Maps of the anatomical locations of the significant positive (red) and negative (blue) correlations with posterior alpha power. All the regions, except for the cluster in the cerebellum ($p=0.07$, corrected) shown here are significant after cluster-level correction for multiple comparisons ($p<0.05$), after passing an uncorrected threshold of $p=0.01$.

comparisons at the cluster level. Clusters were defined as adjacent voxels passing a $p=0.01$ uncorrected threshold.

For comparison, we also performed the same analysis for alpha power extracted from the electrode Pz, which is the electrode at which the average scalp topography of the central posterior electrode is maximal. All the analysis steps for the alpha power estimation at this electrode and regressor construction were the same as for the independent component-based analysis. To investigate how strongly the channel-based and independent component-based alpha regressors are related, the squared partial correlation is computed for each subject. The four compartment signals and the realignment parameters were partialled out.

Functional connectivity analysis

The correlation analysis of the alpha power and the BOLD signal yielded a negative correlation between alpha and

BOLD with the strongest effect observed in the primary visual cortex. As a seed region, the largest significant cluster observed at a voxel-level threshold level of 0.001 was selected. At this threshold, this was the only significant cluster, and it largely falls within the (predominantly right) primary visual cortex (68.3% of the volume of the cluster, anatomy toolbox) (Eickhoff et al., 2005). The realignment parameters and the four compartment signals were included as nuisance variables in the linear model. Multiple comparisons correction was carried out at the cluster level using the Gaussian random field theory after applying an uncorrected voxel-level threshold of $p=0.01$.

EEG modulation of BOLD connectivity: PPI analysis

The modulatory effect of EEG power on BOLD connectivity between the alpha correlation-based seed region in the visual cortex (the same seed as for the connectivity analysis) and the rest of the brain was assessed using a standard PPI approach (Friston et al., 1997). This method is usually used to investigate task-related differences in connectivity between experimental conditions, by testing whether the regression slopes of the (BOLD) signals in different brain regions vary as a function of the task conditions. Here our task variable is the strength of the posterior alpha rhythm, which we divided in two levels (high and low) based on a median split. Connectivity changes, here, are therefore defined as a significant difference in the regression slope between the BOLD signal in the seed region and the rest of the brain as a function of alpha power level.

The seed region in the early visual cortex was based on the negative relation between BOLD and central posterior alpha power. This region was chosen, because the likely source of the central posterior alpha component is located in the primary visual cortex (Makeig et al., 2002, 2004a). We have previously demonstrated that the BOLD signal is negatively correlated with alpha power (Scheeringa et al., 2011). Therefore, this seed is the best choice to investigate how alpha oscillations originating from the early visual cortex modulate its connectivity with other brain regions.

Like the functional connectivity analysis and the alpha-BOLD correlation analysis, the PPI analysis can be formulated in terms of a multiple linear regression. The contents of the design matrix for this regression are graphically depicted in Fig. 4C. The first two regressors of the design matrix interest were formed from the seed BOLD signal in high
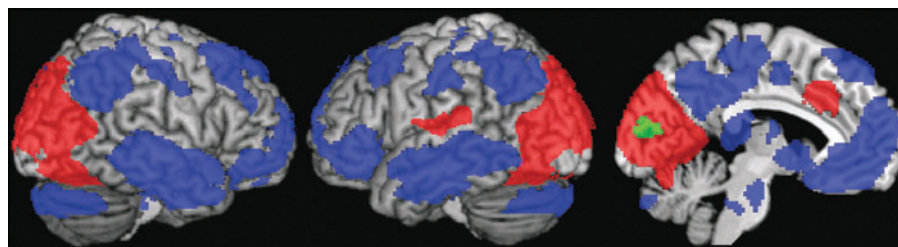

FIG. 3. Functional connectivity maps for a seed region in the primary visual cortex. Positive connections are depicted in red, negative in blue. The same seed region as used for the psychophysiological interaction (PPI) analysis was used here and is shown in green. All the regions shown here are significant after cluster-level correction for multiple comparisons ($p<0.05$), after passing an uncorrected threshold of $p=0.01$.
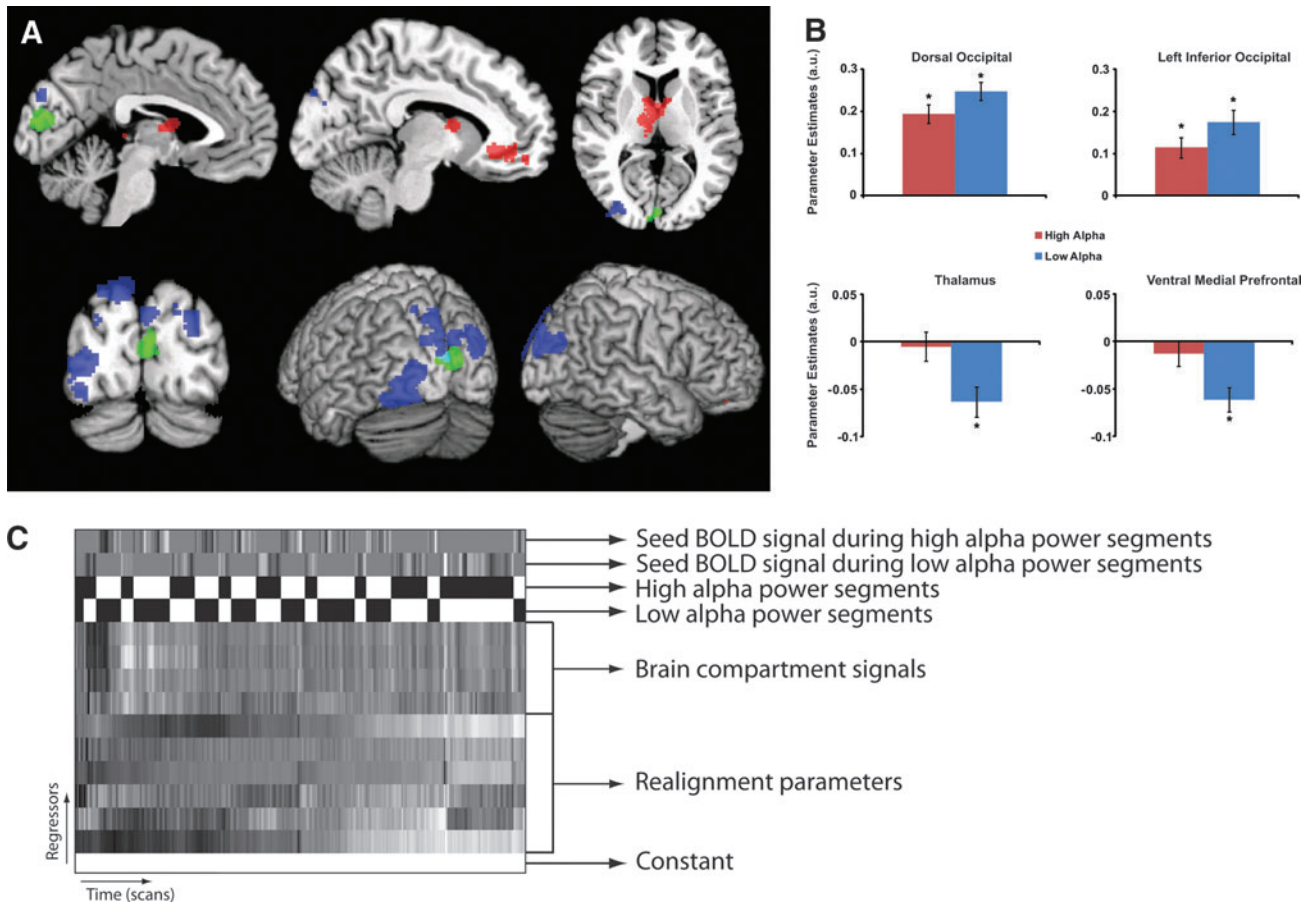
FIG. 4. Results for the PPI analysis. **(A)** Anatomical maps of the contrast estimates for the alpha-based PPI analysis. Red indicates a positive contrast estimate, blue a negative. The seed region is depicted in green. All the negative effects and the positive effect in the thalamus are significant after cluster-level correction for multiple comparisons ($p < 0.05$), after passing an uncorrected threshold of $p = 0.01$. The positive ventral-medial prefrontal cluster is marginally significant ($p = 0.054$, corrected). **(B)** Average parameter estimates for high and low alpha conditions for the significant clusters depicted in **(A)**. *A significant difference from zero ($p < 0.001$). Error bars indicate the standard error of the mean. **(C)** A graphical representation of the design matrix used in the PPI analysis for a typical subject. The contents of the regressors are indicated on the right. For display purposes, the individual regressors are scaled such that the minimum is black and the maximum full white.

or low alpha power conditions. These two regressors of interest form the basis for the PPI analysis. They were constructed by first dividing the alpha power time course into 36 segments with a length of 7 MRI volumes (16.38 s). The EEG segments started 2 volumes (4.68 s) earlier to take into account the delay of the hemodynamic response relative to the underlying neural activity. Subsequently, average alpha power was calculated for each segment. The average alpha power was calculated by averaging the values of the alpha power time course used in the alpha power-BOLD correlation. Subsequently, the segments were divided in high and low alpha segments based on a median split on the average alpha power values per segment (the psychological variable). Two regressors were formed based on this median split. The first consisted of the seed BOLD-signal of segments when alpha power was high and was zero otherwise. The second regressor was constructed in the same way from low alpha power segments. Before these regressors were formed, the seed time course was transformed to reflect the percentage difference from the mean signal. By splitting high and low alpha power up in two regressors, the connectivity maps for low

and high alpha power can be computed separately. Since there were 257 volumes, which is not a multiple of seven, the first five fMRI volumes were not labeled to be either high or low alpha power. Besides these two regressors, two regressors were included in the design matrix that model the mean BOLD signal offset related to the high and low alpha power conditions. The other confound regressors included in the design matrix were the four compartment signals and the motion parameters. At group level, differences in parameter estimates for the high and low alpha power seed signals were tested by means of a dependent sample t-test. Multiple comparison correction was carried out at the cluster level using Gaussian random field theory after applying an uncorrected voxel-level threshold of $p = 0.01$.

Differences found by this comparison are not directly interpretable. For this, we need to know whether the connectivity is negative or positive in the high and low alpha conditions separately. Positive effects, for example, can be caused by a negative coupling becoming weaker (e.g., closer to zero), or a positive coupling becoming stronger when alpha power is high. The reverse logic applies for negative effects. Therefore,

we calculated the mean parameter estimates for high and low alpha segments separately for the significant clusters. These values were tested through single-sample t-tests against zero.

EEG modulation of BOLD connectivity:
frequency specificity of the PPI effects

For the regions in which power in the alpha-band modulated connectivity with the seed, we investigate whether the observed effects are specific for the posterior alpha rhythm or whether they are related to changes in power across a wider frequency range. Although the ICA denoising strategy was optimized for isolating the posterior alpha rhythm, it remains possible that our results are related to leakage from neighboring frequency bands or general broad-band changes in power that include that alpha band. Broad-frequency band power changes have earlier been observed in humans (Miller, 2010), and broad shifts from higher to lower frequencies are thought to be closely related to the BOLD signal (Kilner et al., 2005). If these frequency a-specific effects leak into an independent component modeling the posterior alpha component, they will not be restricted to the alpha band when the ICA unmixing weights are applied on unfiltered data. If this is true, power changes outside the alpha-frequency band are also expected to modulate the connectivity in a similar way. To explicitly investigate this, we first applied the unmixing weights of the selected alpha component to the unfiltered data. By applying the unmixing weights of the alpha IC to the unfiltered data, we apply a spatial filter for activity in other frequency bands that favors a similar underlying source configuration as the alpha rhythm. Subsequently, we applied a time-frequency analysis of power for all frequencies up to 30 Hz, again using two-second Hanning tapered windows that were shifted in 0.1-Hz steps. A 4-Hz spectral smoothing was carried out by computing the average signal over the power time courses between the four bins below and above the center frequency for each frequency bin between 2.5 and 27.5 Hz. Subsequently, for each frequency, a PPI analysis as described in the previous section was performed between the seed region and the average signal in the regions for which connectivity changes were observed in the alpha band. This produces a spectrum that indicates the modulatory effect of power changes on fMRI connectivity between 2.5 and 27.5 Hz.

Significant effects of power on fMRI connectivity were assessed using a nonparametric cluster-based randomization procedure that effectively controls the type 1 error rate in a situation involving multiple comparisons (Maris and Oostenveld, 2007). This randomization procedure allows for the construction of user-defined test statistics tailored to the effect of interest within the framework of a cluster-based randomization test. It works by calculating the sum of a statistic of choice over all data points within a cluster that exceeds an arbitrary predefined threshold. Each cluster sum is then compared with a distribution of maximum cluster sums obtained by randomly permuting the labels of the independent variable. Clusters that fall within the upper or lower 2.5% of the randomization distribution were considered significant. The number of randomizations for computing the reference distribution was set to 10,000. For the effect of alpha power on BOLD connectivity, we used the t-value obtained by the dependent-samples t-test between parameter estimates for the high and low alpha power seed region regressors. Clusters were defined as adjacent frequency bins exceeding an uncorrected p-value of 0.01 for this t-test.

Since the unmixing weights were estimated on alpha band-filtered data, the ICA component was partly selected on the presence of an alpha peak in the spectrum, and the brain regions for which the frequency-specific effects were computed were based on the presence of an alpha effect; this analysis is not intended to show that effects and other frequency bands do not modulate BOLD–BOLD connectivity between regions. This analysis is carried out to investigate whether the observed effects here are related to the central posterior alpha rhythm or if they are related to frequency a-specific effects. Regions that do not show alpha band-modulated connectivity and are therefore not included here might show a modulation with other or broader frequency ranges, and other sources with different frequency characteristics that do not pass the spatial filter provided by the alpha component might still modulate connectivity between the regions studied here.

Results

Alpha-BOLD correlation

The maps for the correlation between alpha power and BOLD are shown in Fig. 2. A large negative cluster is located in the early visual cortex ($k = 3776, p = 1.4 \times 10^{-13}$, corrected for multiple comparisons) with its maximum located in the right extrastriate cortex (location according to the coordinate system of the Montreal Neurological Institute (MNI): 30, −92, 22; $z = 3.79$) and a second strong local maximum in the primary visual cortex (MNI coordinates: 2, −88, 10; $z = 3.78$). A second marginally significant cluster is observed in the left cerebellum (MNI coordinates: −32, −38, −36; $k = 365$; $z = 3.80$; $p = 0.070$)

The strongest positive correlations are observed in the posterior cingulate/precuneus (MNI coordinates: 6, −62, 28; $k = 1294$; $z = 5.25$; $p = 5.2 \times 10^{-6}$). Other positive correlations were observed in the medial prefrontal cortex (MNI coordinates: 0, 56, −10; $k = 6230$; $z = 5.05$; $p < 1 \times 10^{-14}$), the left lateral inferior parietal cortex (MNI coordinates: −38, −82, 38; $k = 600$; $z = 3.94$; $p = 0.004$) and the left (MNI coordinates: −56, −14, −12; $k = 903$; $z = 4.95$; $p = 1.8 \times 10^{-4}$) and the right (MNI coordinates: 64, −12, −16; $k = 480$; $z = 4.61$; $p = 0.017$) middle temporal gyrus and the right cerebellum (MNI coordinates: 34, −54, −32; $k = 513$; $z = 3.32$; $p = 0.011$). Except for the cerebellum, these positively correlating regions are all part of or associated with the default mode network (DMN) (Raichle et al., 2001; Raichle and Snyder, 2007; Shulman et al., 1997).

For comparison, we performed the same analysis using the electrode Pz as the basis for the alpha–BOLD correlation. The squared partial correlation between the Pz-based and independent component-based regressors was 0.495 (s = 0.325), indicating circa 50% of the variances is not shared. Supplementary Fig. S1A (Supplementary Data are available online at www.liebertpub.com/brain) demonstrates that the strength of the squared partial correlation varies strongly over subjects. All normal partial correlations were positive. While for seven subjects, squared partial correlations larger than 0.8 were observed, other subjects showed substantially lower values. This indicates that compared to other brain and noise sources the relative strength at which the posterior

alpha component is expressed at the electrode Pz varies considerably over subjects. The comparison for the whole-brain correlational analysis for the two regressors is depicted in Supplementary Fig. S1B. This figure demonstrates there is considerable overlap between the two approaches. When, however, viewed in more detail, it demonstrates that the independent component-based alpha regressor is associated with a larger area of negative correlations in the primary visual cortex than the channel-based regressor, while the reversed pattern is observed for negative correlations outside the primary visual cortex. This suggests that the alpha power fluctuations in the selected independent component are more closely related to the primary visual cortex than fluctuations at the channel level.

Functional connectivity

The maps for the functional connectivity with the (alpha-based) seed in the primary visual cortex are depicted in Fig. 3. Positive correlations with the seed regions are observed across a large part of the occipital lobe, encompassing both striate and extrastriate visual regions. In addition, positive clusters are observed in the dorsal anterior cingulate cortex and the left temporal–parietal junction. In contrast, negative correlations are observed in the posterior cingulate cortex/precuneus, the medial frontal cortex, lateral inferior parietal cortices, left and right middle temporal gyrus, bilateral inferior frontal cortices, bilateral hippocampus, and bilateral supplementary motor areas. Thus, these regions comprise the full extent of the DMN, and additional areas.

PPI analysis

The results for the PPI analysis are depicted in Fig. 4. The largest cluster with a negative effect was observed bilaterally in the dorsal part of the occipital lobe, largely within area V3/V3A (superior and middle occipital gyrus, MNI coordinates: $-18, -88, 42; k = 665; z = 4.59; p = 0.001$). A second cluster with a negative effect was observed in the left inferior occipital cortex, partly overlapping with area V4 (Fusiform and middle occipital gyrus, BA19, MNI coordinates: $-34, -70, -18$; $k = 583; z = 3.44; p = 0.003$).

Two regions showing a (marginally) significant positive effect were observed. The first region was observed in the medial and anterior thalamus (MNI coordinates: $-4, -4, 10$; $k = 407; z = 4.49; p = 0.026$). The second cluster was observed in the ventral-medial part of the prefrontal cortex (BA32, MNI coordinates: $18, 46, -10; k = 352; z = 3.81; p = 0.054$).

To interpret the effects, we need to take into account the signs of the effects in the high and low alpha power conditions. The average parameter estimates for the observed clusters for both conditions are depicted in Fig. 4B. These results indicate that for the clusters, where the parameter estimates in the high alpha condition are lower than in the low alpha condition (blue clusters in Fig. 4A), there is positive connectivity between the seed and the clusters for both high and low alpha power conditions. The difference, therefore, indicates that for these clusters connectivity strength is lower in the high alpha condition compared to the low alpha condition. For the two positive clusters (red clusters in Fig. 4A) we see that for the low alpha condition coupling with the seed region is negative. In the high alpha power condition, this negative coupling is, however, virtually absent. Here

the parameter estimates do not significantly differ from zero. For all four clusters, the results seem to indicate that the coupling strength with the seed region decreases when alpha power increases, irrespective of whether there is a positive or negative coupling with the seed region.

To test whether the effects are specific to the alpha band, or whether the effects are related to power changes over a wider frequency range, we repeated the PPI analysis for all frequencies between 2.5 and 27.5 Hz in the observed regions. The results are depicted in Fig. 5. For all four regions, the effect is clearly the strongest in the alpha band and for all four regions only the effects in this band are significant after correction for multiple comparisons. This indicates that the effects found for these regions are specifically related to alpha power variations, and not related to broad-band power changes. Note that the effects in the alpha band depicted in Fig. 5 are likely inflated by selecting only significant clusters from the whole-brain analysis.

Discussion

In this experiment, we studied how the resting-state connectivity within the visual system and between the visual system and other brain regions is modulated as a function of posterior alpha power. We observed that the increased local alpha synchronization, as indexed by an increase in power, originating from the early visual cortex is associated with decreased fMRI resting-state connectivity within the visual system. In addition, the negative coupling with the anterior and medial thalamus and the ventral medial prefrontal cortex was reduced in strength with increased alpha power. Furthermore, these reductions in connectivity strength were found to be specific for the alpha-frequency range.

The fact that alpha-band neuronal synchronization is inversely related to connectivity between the primary visual cortex and closely connected regions (Felleman and Van Essen, 1991) in both the dorsal and ventral visual stream regions suggests that local alpha-band synchronization serves to reduce the communication between closely connected regions. This notion is in line with a general functional role of alpha-band synchronization in inhibiting spurious activity, as suggested by the alpha inhibition hypothesis proposed by Klimesch and colleagues (2007). In addition, our results suggest that, not only activity within visual regions is decreased when the level of alpha synchronization is high, as evidenced through the BOLD-power correlation analysis here and earlier by others (de Munck et al., 2009; Goldman et al., 2002; Laufs et al., 2003a; Mantini et al., 2007; Moosmann et al., 2003; Scheeringa et al., 2009, 2011), but that as a consequence, also connectivity and communication with tightly connected brain regions is reduced, as shown by the PPI analysis. This could be related to the notion that alpha oscillations are thought to be related to feed-back processes in the deeper cortical layers (Bollimunta et al., 2008, 2011; Buffalo et al., 2011; Maier et al., 2010, 2011), that affect gamma-band activity (Osipova et al., 2008) which has predominantly been associated with activity in superficial cortical layers (Buffalo et al., 2011; Maier et al., 2010, 2011). Superficial cortical layers are thought to be involved in feed-forward connections to higher order visual regions (Douglas and Martin, 2004; Gilbert, 1983). Stronger alpha oscillations could provide stronger inhibition to superficial layer feed-forward connections that
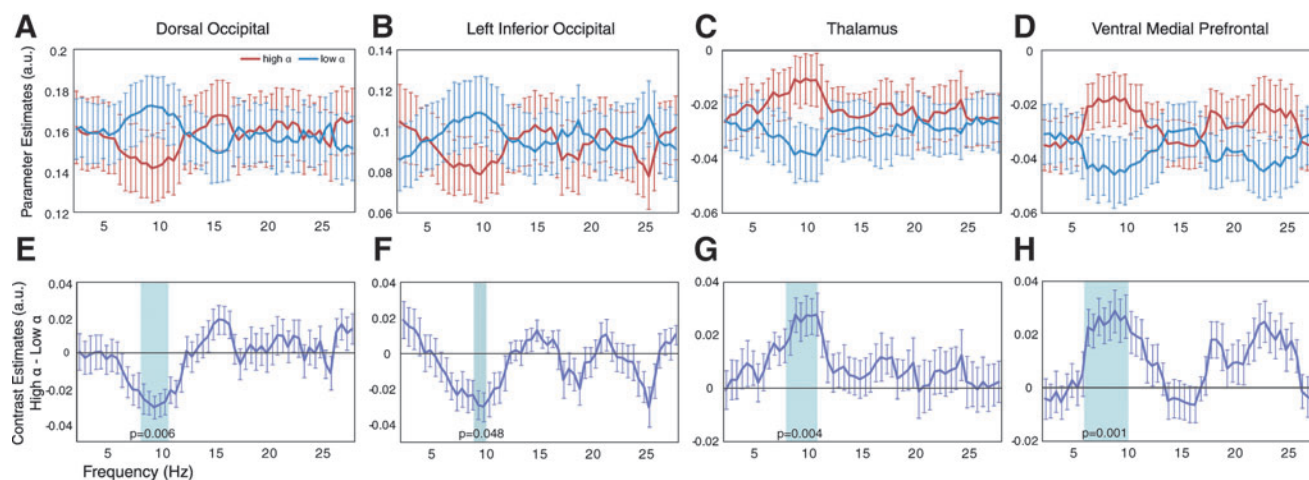
FIG. 5. Results for the frequency-specific PPI effects for the observed significant clusters for the whole-brain alpha power PPI analysis. **(A–D)** For each cluster, the parameter estimates for the high and low alpha condition for frequencies between 2.5 and 27.5 Hz are shown. **(E–H)** The differences between the two conditions are shown. The shaded area indicates this difference deviates significantly from zero after multiple comparisons correction. For all panels, error bars indicate the standard error of the mean. Indicated *p*-values are corrected for multiple comparisons using a nonparametric cluster-based correction method. Note that the values in **(A–D)** are mirrored around the mean-level connectivity the different regions have with the seed. This is caused by the fact that the same seed signal segments are sorted into high- and low-power categories for each separate frequency bin.

would result in the reduced connectivity with higher order visual regions we observed here. Based on our results we, however, cannot distinguish between feed-forward and feed-back effects.

It is unlikely that the observed effects are related to smaller fluctuations in alpha power that do not exceed the high- versus low-power cutoff. This would first assume that the posterior alpha rhythm we study here is generated and has a widely distributed source in both the seed regions as well as the more distant higher order visual regions. The most likely source location of this rhythm is, however, found in the primary visual cortex (Makeig et al., 2004a, 2004b) and not in the higher order visual regions for which connectivity is changed as a function of alpha power. Furthermore, if these regions do contribute to the observed changes in alpha power, it is unlikely that this is related to the observed PPI effect. This would not only assume that the transfer function from alpha oscillations to the BOLD signal is different for the seed and the regions that show a alpha-modulated connectivity change with the seed, but also that this difference is different for the high and low alpha power conditions.

The frequency resolved analysis for the regions that showed a change in connectivity with the seed as a function of by alpha-band power demonstrated that this effect was indeed limited to the alpha band. This demonstrates that the connectivity changes for these regions are not related to broad-band changes in power (Miller, 2010) or a general shift from high- to low-frequency activity (Kilner et al., 2005) that also happens to manifest themselves in the alpha band. The fact that no effects were observed for the neighboring theta and beta bands strongly suggests that they are directly related to changes in local alpha-band synchronization. By selecting the central posterior alpha component and restricting the analysis to only the regions that showed a PPI effect for alpha power, these results, however, only demonstrate that the observed connectivity effects are indeed re-

lated to alpha power changes. Based on this analysis, we cannot exclude that power changes in other modulates the connectivity from the seed with other brain regions. This analysis does also not exclude that sources with a different projection to the scalp, and therefore at least partly different underlying neural sources, show modulatory effects of power changes in other frequency bands on connectivity between the primary visual cortex and the brain regions observed here.

The gamma frequency range (30–100 Hz) was not investigated here, and effects of the gamma activity on fMRI connectivity can therefore not be ruled out. We recently demonstrated that gamma-band oscillations can be measured in the MRI environment and are related to the BOLD signal (Scheeringa et al., 2011). These gamma-band effects were, however, directly related to visual stimulation, and cannot reliably be measured from the visual cortex with EEG in a resting-state context. In addition, the EEG for this previous study was measured in between the acquisition of fMRI volumes. Therefore, the gamma band was not compromised by the presence of residual artefacts related to the radio-frequency pulse and switching of the magnetic gradient. The fMRI data presented here were recorded without gaps that allow for gradient-free EEG recording. Since gamma oscillations are relatively small compared to the residual gradient artifacts in the gamma range, and gamma-band activity from the visual cortex cannot be reliably measured in resting state, our data are not suited to study connectivity changes as a function of gamma power changes.

Our observation that increased alpha-band synchrony, as indexed by increased power, is related to decreased connectivity and seems to contradict the idea that neural synchronization serves functional integration (Fries, 2009; Kahana et al., 2001; Palva and Palva, 2007; Varela et al., 2001). It is, however, important to consider that the most likely source location of the central posterior alpha component lies within the

primary visual cortex (Makeig et al., 2004a, 2004b), and the reduced connectivity is within the surrounding extrastriate regions. This strongly suggests that local increases in synchrony in the alpha band are related to decreased communication with regions that are strongly connected, but farther removed.

For two brain regions, the anterior and medial thalamus and the ventromedial prefrontal cortex, posterior alpha power modulated their antagonistic relation with the seed in the primary visual cortex. In both cases, this antagonistic relation was weaker or absent when the alpha power is high. Both regions have been related to memory processing. The anterior nucleus of the thalamus has extensive connections with the hippocampus and lesions here have resulted in amnesic syndromes (Aggleton and Brown, 1999). The ventromedial prefrontal cortex, which was found marginally significant, has been found to coactivate with the hippocampus (Vincent et al., 2006) and has also been closely related to memory (van Kesteren et al., 2012). Whenever the primary visual cortex is disengaged from processing external visual information, which is reflected in a relatively high alpha power, it interacts stronger with systems processing internal memory representations. This could explain the inverse relation between the visual cortex and these two memory regions. Our results suggest this inverse relation might be modulated by the strength of alpha oscillations, in the sense that this inverse relation becomes progressively stronger when power increases. This would fit within a recently proposed framework suggesting that alpha oscillations bias the brain toward processing information from internal or external sources (Hanslmayr et al., 2011a).

The most significant cluster with a positive PPI effect was found in the anterior and medial thalamus. This might be surprising since the thalamus is thought to be strongly related to the generation of alpha oscillations, which would more likely result in stronger (e.g., more negative) coupling between the thalamus and the primary visual cortex. This role in alpha generation, however, is more likely related to the lateral geniculate and the thalamic reticular nuclei (Hughes and Crunelli, 2005; Saalmann and Kastner, 2011). These regions were not part of the significant cluster we observed.

The most parsimonious interpretation of the results presented here is that increased strength of alpha oscillations in the early visual cortex is related to a decrease in coupling of that region with other brain regions. This can decrease positive coupling, but also decrease antagonistic coupling with another brain region. Alpha oscillations have been observed outside the visual system (e.g., the somatosensory mu rhythm), and we hypothesize this pattern is similar across the brain. Whether this facilitates or impairs task performance will depend on the task context. In contexts, where increased alpha power predicts impaired performance (Mazaheri et al., 2009), we expect that this is related to decreased connectivity between task-relevant regions. Increased task performance has also been related to increased strength of alpha oscillations (Haegens et al., 2010; Scheeringa et al., 2009). We expect that this effect is related to decreased connectivity of task-irrelevant regions with other task-relevant regions.

Most studies using simultaneously recorded EEG and fMRI have related changes in EEG power measures to changes in the level of the BOLD signal (de Munck et al., 2009; Goldman et al., 2002; Laufs et al., 2003a, 2003b; Mantini et al., 2007; Moosmann

et al., 2003; Sammer et al., 2007; Scheeringa et al., 2008, 2009, 2011). This work presents an initial report of changes in the strength of fMRI connectivity that correlate with changes in measures of local neuronal synchronization (here alpha power). Until now, analyses of fMRI resting-state data have employed a rather static view on connectivity. Our work demonstrates a more dynamic view that can potentially lead to new insights and as such, it is more in line with De Pasquale and colleagues (2010) who studied the temporal dynamics of resting-state networks in magnetoencephalography. Our approach of combining EEG- and fMRI-based measures for studying dynamic network coupling can readily be extended to power changes in other frequencies, EEG features, neural sources, and brain networks, both under task or resting-state conditions. It therefore opens up new avenues for investigating the dynamics of functional networks at potentially more detailed temporal and spatial scales than can be obtained by either technique alone.

Author Disclosure Statement

No competing financial interests exist.

References

Aggleton JP, Brown MW. 1999. Episodic memory, amnesia, and the hippocampal-anterior thalamic axis. Behav Brain Sci 22:425–444; discussion 444–489.

Allen PJ, Josephs O, Turner R. 2000. A method for removing imaging artifact from continuous EEG recorded during functional MRI. Neuroimage 12:230–239.

Allen PJ, Polizzi G, Krakow K, Fish DR, Lemieux L. 1998. Identification of EEG events in the MR scanner: the problem of pulse artifact and a method for its subtraction. Neuroimage 8: 229–239.

Ashburner J, Friston KJ. 2005. Unified segmentation. Neuroimage 26:839–851.

Biswal B, Yetkin FZ, Haughton VM, Hyde JS. 1995. Functional connectivity in the motor cortex of resting human brain using echo-planar MRI. Magn Reson Med 34:537–541.

Bollimunta A, Chen Y, Schroeder CE, Ding M. 2008. Neuronal mechanisms of cortical alpha oscillations in awake-behaving macaques. J Neurosci 28:9976–9988.

Bollimunta A, Mo J, Schroeder CE, Ding M. 2011. Neuronal mechanisms and attentional modulation of corticothalamic alpha oscillations. J Neurosci 31:4935–4943.

Buffalo EA, Fries P, Landman R, Buschman TJ, Desimone R. 2011. Laminar differences in gamma and alpha coherence in the ventral stream. Proc Natl Acad Sci U S A 108:11262–11267.

Damoiseaux JS, Rombouts SARB, Barkhof F, Scheltens P, Stam CJ, Smith SM, Beckmann CF. 2006. Consistent resting-state networks across healthy subjects. Proc Natl Acad Sci U S A 103:13848–13853.

de Munck JC, Goncalves SI, Mammoliti R, Heethaar RM, Lopes da Silva FH. 2009. Interactions between different EEG frequency bands and their effect on alpha-fMRI correlations. Neuroimage 47:69–76.

De Pasquale F, Della Penna S, Snyder AZ, Lewis C, Mantini D, Marzetti L, Belardinelli P, Ciancetta L, Pizzella V, Romani GL, Corbetta M. 2010. Temporal dynamics of spontaneous MEG activity in brain networks. Proc Natl Acad Sci U S A 107:6040–6045.

Debener S, Ullsperger M, Siegel M, Engel AK. 2006. Single-trial EEG-fMRI reveals the dynamics of cognitive function. Trends Cogn Sci 10:558–563.

Delorme A, Makeig S. 2004. EEGLAB: an open source toolbox for analysis of single-trial EEG dynamics including independent component analysis. J Neurosci Methods 134:9–21.

Douglas RJ, Martin KA. 2004. Neuronal circuits of the neocortex. Annu Rev Neurosci 27:419–451.

Eickhoff SB, Stephan KE, Mohlberg H, Grefkes C, Fink GR, Amunts K, Zilles K. 2005. A new SPM toolbox for combining probabilistic cytoarchitectonic maps and functional imaging data. Neuroimage 25:1325–1335.

Felleman DJ, Van Essen DC. 1991. Distributed hierarchical processing in the primate cerebral cortex. Cereb Cortex 1:1–47.

Fox MD, Snyder AZ, Vincent JL, Corbetta M, Van Essen DC, Raichle ME. 2005. The human brain is intrinsically organized into dynamic, anticorrelated functional networks. Proc Natl Acad Sci U S A 102:9673–9678.

Fries P. 2009. Neuronal gamma-band synchronization as a fundamental process in cortical computation. Annu Rev Neurosci 32:209–224.

Friston KJ, Buechel C, Fink GR, Morris J, Rolls E, Dolan RJ. 1997. Psychophysiological and modulatory interactions in neuroimaging. Neuroimage 6:218–229.

Friston KJ, Harrison L, Penny W. 2003. Dynamic causal modelling. Neuroimage 19:1273–1302.

Gilbert CD. 1983. Microcircuitry of the visual cortex. Annu Rev Neurosci 6:217–247.

Goldman RI, Stern JM, Engel J, Cohen MS. 2002. Simultaneous EEG and fMRI of the alpha rhythm. Neuroreport 13:2487–2492.

Haegens S, Osipova D, Oostenveld R, Jensen O. 2010. Somatosensory working memory performance in humans depends on both engagement and disengagement of regions in a distributed network. Hum Brain Mapp 31:26–35.

Hanslmayr S, Gross J, Klimesch W, Shapiro KL. 2011a. The role of alpha oscillations in temporal attention. Brain Res Rev 67:331–343.

Hanslmayr S, Volberg G, Wimber M, Raabe M, Greenlee MW, Bauml KH. 2011b. The relationship between brain oscillations and BOLD signal during memory formation: a combined EEG-fMRI study. J Neurosci 31:15674–15680.

Hoogenboom N, Schoffelen JM, Oostenveld R, Parkes LM, Fries P. 2006. Localizing human visual gamma-band activity in frequency, time and space. Neuroimage 29:764–773.

Hughes SW, Crunelli V. 2005. Thalamic mechanisms of EEG alpha rhythms and their pathological implications. Neuroscientist 11:357–372.

Kahana MJ, Seelig D, Madsen JR. 2001. Theta returns. Curr Opin Neurobiol 11:739–744.

Kilner JM, Mattout J, Henson R, Friston KJ. 2005. Hemodynamic correlates of EEG: a heuristic. Neuroimage 28:280–286.

Klimesch W, Sauseng P, Hanslmayr S. 2007. EEG alpha oscillations: the inhibition-timing hypothesis. Brain Res Rev 53:63–88.

Laufs H, Kleinschmidt A, Beyerle A, Eger E, Salek-Haddadi A, Preibisch C, Krakow K. 2003a. EEG-correlated fMRI of human alpha activity. Neuroimage 19:1463–1476.

Laufs H, Krakow K, Sterzer P, Eger E, Beyerle A, Salek-Haddadi A, Kleinschmidt A. 2003b. Electroencephalographic signatures of attentional and cognitive default modes in spontaneous brain activity fluctuations at rest. Proc Natl Acad Sci U S A 100:11053–11058.

Lee TW, Girolami M, Sejnowski TJ. 1999. Independent component analysis using an extended infomax algorithm for mixed subgaussian and supergaussian sources. Neural Comput 11:417–441.

Maier A, Adams GK, Aura C, Leopold DA. 2010. Distinct superficial and deep laminar domains of activity in the visual cortex during rest and stimulation. Front Syst Neurosci 4: p ii 31.

Maier A, Aura CJ, Leopold DA. 2011. Infragranular sources of sustained local field potential responses in macaque primary visual cortex. J Neurosci 31:1971–1980.

Makeig S, Debener S, Onton J, Delorme A. 2004a. Mining event-related brain dynamics. Trends Cogn Sci 8:204–210.

Makeig S, Delorme A, Westerfield M, Jung TP, Townsend J, Courchesne E, Sejnowski TJ. 2004b. Electroencephalographic brain dynamics following manually responded visual targets. PLoS Biol 2:e176.

Makeig S, Westerfield M, Jung TP, Enghoff S, Townsend J, Courchesne E, Sejnowski TJ. 2002. Dynamic brain sources of visual evoked responses. Science 295:690–694.

Mantini D, Perrucci MG, Del Gratta C, Romani GL, Corbetta M. 2007. Electrophysiological signatures of resting state networks in the human brain. Proc Natl Acad Sci U S A 104:13170–13175.

Maris E, Oostenveld R. 2007. Nonparametric statistical testing of EEG- and MEG-data. J Neurosci Methods 164:177–190.

Mazaheri A, Jensen O. 2010. Rhythmic pulsing: linking ongoing brain activity with evoked responses. Front Hum Neurosci 4:177.

Mazaheri A, Nieuwenhuis IL, van Dijk H, Jensen O. 2009. Prestimulus alpha and mu activity predicts failure to inhibit motor responses. Hum Brain Mapp 30:1791–1800.

Miller KJ. 2010. Broadband spectral change: evidence for a macroscale correlate of population firing rate? J Neurosci 30:6477–6479.

Moosmann M, Ritter P, Krastel I, Brink A, Thees S, Blankenburg F, Taskin B, Obrig H, Villringer A. 2003. Correlates of alpha rhythm in functional magnetic resonance imaging and near infrared spectroscopy. Neuroimage 20:145–158.

Oostenveld R, Fries P, Maris E, Schoffelen JM. 2011. FieldTrip: open source software for advanced analysis of MEG, EEG, and invasive electrophysiological data. Comput Intell Neurosci 2011:156869.

Osipova D, Hermes D, Jensen O. 2008. Gamma power is phase-locked to posterior alpha activity. PLoS One 3:e3990.

Palva S, Palva JM. 2007. New vistas for alpha-frequency band oscillations. Trends Neurosci 30:150–158.

Pfurtscheller G, Stancak A, Jr., Neuper C. 1996. Event-related synchronization (ERS) in the alpha band—an electrophysiological correlate of cortical idling: a review. Int J Psychophysiol 24:39–46.

Raichle ME, MacLeod AM, Snyder AZ, Powers WJ, Gusnard DA, Shulman GL. 2001. A default mode of brain function. Proc Natl Acad Sci U S A 98:676–682.

Raichle ME, Snyder AZ. 2007. A default mode of brain function: a brief history of an evolving idea. Neuroimage 37:1083–1090.

Saalmann YB, Kastner S. 2011. Cognitive and perceptual functions of the visual thalamus. Neuron 71:209–223.

Sammer G, Blecker C, Gebhardt H, Bischoff M, Stark R, Morgen K, Vaitl D. 2007. Relationship between regional hemodynamic activity and simultaneously recorded EEG-theta associated with mental arithmetic-induced workload. Hum Brain Mapp 28:793–803.

Scheeringa R, Bastiaansen MC, Petersson KM, Oostenveld R, Norris DG, Hagoort P. 2008. Frontal theta EEG activity correlates negatively with the default mode network in resting state. Int J Psychophysiol 67:242–251.

Scheeringa R, Fries P, Petersson KM, Oostenveld R, Grothe I, Norris DG, Hagoort P, Bastiaansen MC. 2011. Neuronal dynamics underlying high- and low-frequency EEG oscillations contribute independently to the human BOLD signal. Neuron 69:572–583.

Scheeringa R, Petersson KM, Oostenveld R, Norris DG, Hagoort P, Bastiaansen MC. 2009. Trial-by-trial coupling between EEG and BOLD identifies networks related to alpha and theta EEG power increases during working memory maintenance. Neuroimage 44:1224–1238.

Shulman GL, Fiez JA, Corbetta M, Buckner RL, Miezin FM, Raichle ME, Petersen SE. 1997. Common blood flow changes across visual tasks .2. Decreases in cerebral cortex. J Cogn Neurosci 9:648–663.

van Kesteren MT, Ruiter DJ, Fernandez G, Henson RN. 2012. How schema and novelty augment memory formation. Trends Neurosci 35:211–219.

Varela F, Lachaux JP, Rodriguez E, Martinerie J. 2001. The brainweb: phase synchronization and large-scale integration. Nat Rev Neurosci 2:229–239.

Vincent JL, Snyder AZ, Fox MD, Shannon BJ, Andrews JR, Raichle ME, Buckner RL. 2006. Coherent spontaneous activity identifies a hippocampal-parietal memory network. J Neurophysiol 96:3517–3531.

Address correspondence to:
René Scheeringa
Donders Institute for Brain, Cognition and Behaviour
Centre for Cognitive Neuroimaging
Radboud University Nijmegen
P.O. Box 9101
6500 HB Nijmegen
The Netherlands

E-mail: rene.scheeringa@donders.ru.nl